
Computation of Aeroacoustic Waves with High Order Spectral Volume Method

Z.J. Wang

Michigan State University, East Lansing, MI 48824, U.S.A

Abstract. A recently developed high-order finite volume method named the spectral volume (SV) method is employed to solve several benchmark problems from the Fourth Computational Aeroacoustics (CAA) Workshop on Benchmark Problems. In particular, the computational results for multiple cylinder wave scattering problems are presented, and compared with analytical solutions. It is shown that a 4th order SV scheme with an equivalent 13 points-per-wave is capable of producing numerical solutions which agree well with analytical solutions.

1 Introduction

A new high-order finite volume (FV) method named the spectral volume (SV) method has been developed recently for hyperbolic conservation laws, and successfully demonstrated for both scalar and system conservation laws [1-4]. The SV method is a Godunov-type finite volume method [5], which has been under development for over three decades, and has become the-state-of-the-art for the numerical solution of hyperbolic conservation laws. The SV method is also related to the discontinuous Galerkin (DG) method [6] and the k-exact FV method [7]. For a review of the literature on the Godunov-type FV and DG methods, refer to [1], and the references therein.

In this study, the SV method is evaluated for several problems in the Fourth Computational Aeroacoustics (CAA) Workshop on Benchmark Problems. As pointed out by Tam in [8], acoustic waves have their own characteristics which make their computation unique and challenging. Acoustic waves are inherently unsteady. Their amplitudes are several orders smaller than the magnitudes of the mean flow and their frequencies are generally very high and broad ranging. Computational methods with high order accuracy are required to capture the acoustic portion of the solution.

The paper is organized as follows. In the next section, the basic formulation of the SV method is reviewed. In Section 3, solutions for the benchmark problems are presented. Conclusions are summarized in Section 4.

2 Spectral (Finite) Volume Method

In the present study, the non-linear Euler equations are employed, which can be expressed as

$$\frac{\partial Q}{\partial t} + \frac{\partial E}{\partial x} + \frac{\partial F}{\partial y} = S, \quad (1a)$$

$$S = \begin{bmatrix} 0 \\ 0 \\ 0 \\ e^{-ln2 \frac{x^2+y^2}{0.2^2}} Sin(\omega t) \end{bmatrix}. \quad (1b)$$

In (1a) Q is the vector of conserved variables, E and F are the inviscid flux vectors in x and y directions respectively and S is the time dependent source term. The governing equation can be cast into the following divergence form

$$\frac{\partial Q}{\partial t} + \nabla \cdot f = S, \quad (2)$$

where $f = (E, F)$. Assume that equations (1a) and (1b) are solved in the computational domain Ω subject to proper initial and boundary conditions. The domain is discretized into N non-overlapping simplex elements (triangular elements in 2D) called spectral volumes (SVs) $\Omega = \cup_i^N S_i$. In order to support a degree k polynomial reconstruction within each SV, the SV is further partitioned into m subcells, with $m = (k+1)(k+2)/2$. Note that m is also the dimension of P^k , the space of polynomials of degree at most k . Many candidate partitions are evaluated in [2]. It was found that the partitions for various k shown in Figure 1 perform satisfactorily. Denote the j^{th} CV of S_i by C_{ij} . In the SV method, the degrees-of-freedom (DOFs) or unknowns are the cell-averaged conservative variable Q at the subcells, or the CVs. Given the DOFs \bar{Q}_{ij} , a polynomial $p_i \in P^k$ can be reconstructed such that it is a $(k+1)$ -th order accurate approximation to the solution Q inside S_j . The reconstruction can be conveniently expressed as

$$p_i(\mathbf{r}) = \sum_{j=1}^m L_j(\mathbf{r}) \bar{Q}_{ij}, \quad (3)$$

where $L_j(\mathbf{r}) \in P^k$ are the "shape" functions shape functions, which are given in [4] for 2D reconstructions. The high-order reconstruction is then used to generate high-order updates for the DOFs using the usual FV method. Integrating (2) in C_{ij} , we obtain the following integral equation for the DOFs

$$\frac{d\bar{Q}_{ij}}{dt} + \frac{1}{V_{ij}} \sum_{r=1}^K \int_{A_r} (\mathbf{f} \cdot \mathbf{n}) dA = \frac{1}{V_{ij}} \int_{C_{ij}} S dV, \quad (4)$$

where K is the number of faces in C_{ij} and A_r represents the r^{th} face of C_{ij} . The surface and volume integrals on each face are performed with Gauss quadrature formulas which are exact for degree k polynomials. The flux vectors at the quadrature points $\mathbf{r}_{r,q}$ are computed with a Riemann solver

$$\mathbf{f}(Q(\mathbf{r}_{rq})) \cdot \mathbf{n} \approx \hat{f}(Q_L(\mathbf{r}_{rq}), Q_R(\mathbf{r}_{rq}), \mathbf{n}), \quad (5)$$

where Q_L and Q_R are the vector of conserved variables just to the left and right of the interface. A third-order TVD Runge-Kutta scheme is employed for time integration [9].

3 Numerical Results

3.1 Category 2 Problem 1 Two Cylinder Wave Diffraction Problem

The scattering of a periodic acoustic source from two circular cylinders is considered. The acoustic source used in this case has a transient term expressed in the following form

$$S = e^{-\ln 2 \frac{x^2 + y^2}{0.25}} \text{Sin}(\omega t) f(t),$$

$$f(t) = \min\left(1, \frac{t^3}{t_0}\right).$$

The following parameters are chosen in the present study: $\omega = 8\pi$, $t_0 = 4$. Since the configuration is symmetric, only the upper half of the physical domain is used in the computation. The computational mesh is displayed in Figure 2a. The entire computational domain extends to $r = 15$. The grid within $r = 9$ is nearly uniform with a mesh size = 0.06. Since each triangle is further partitioned into 10 subcells, the grid has an equivalent points-per-wave (PPW) of about 13 ($\sqrt{10} * 0.25 / 0.06$). The mesh is coarsened from $r = 9$ to $r = 15$ with an expansion factor of 1.1 to serve as the buffer zone. A constant time step of 0.002 was used in the computation with a total of 20,000 time steps. The 4th order SV scheme was employed in the computation. The rms pressure is computed in the last 2000 time steps. The computed pressure field at a certain time is shown in Figure 2b. Note that the outgoing waves are significantly damped in the buffer zone without visible reflections. The computed rms pressure along the center line is compared with the analytical solution [10] in Figure 3. The rms pressure on the two cylinder surfaces is also compared with the analytical solution in Figure 4. Note that the agreement between the computational and analytical solutions is good with the current grid resolution.

3.2 Problem 2 Three Cylinder Wave Diffraction Problem

The flow conditions are similar to the last problem. The only difference is the geometry. The computational grid is shown in Figure 5a. The mesh has an inner zone inside $r = 9$, and an outer buffer zone from $r = 9$ to $r = 14$. The inner zone has a grid size of 0.06. The mesh is coarsened from $r = 9$ to $r = 14$ with an expansion factor of 1.1 to serve as the buffer zone. The computed pressure field is shown in Figure 5b. The computed rms pressure along the center line is compared with the analytical solution in Figure 6. The rms pressure on the two

cylinder surfaces is also compared with the analytical solution in Figure 7. Note again that there is a good agreement between the computational and analytical solutions.

4 CONCLUSIONS

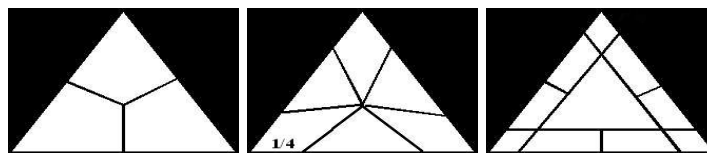
The SV method has been tested on two benchmark problems in the Fourth Computational Aeroacoustics (CAA) Workshop on Benchmark Problems. For the Category 2 problems, the 4th SV scheme was capable of producing reasonable results with a grid resolution of about 13 PPW. The advantage of the SV method lies in its capability of handling complex geometries in a very flexible manner. The problems can all be set up in minutes.

Acknowledgements

Some of the work presented in the paper was conducted while the author was visiting the Air Force Research Laboratory, Dayton with support from the AFRLs summer faculty program. The author thanks Drs. Miguel Visbal and Scott Sherer for many helpful discussions and for providing the analytical solutions for the Category 2 problems.

References

1. Wang, Z.J.: *J. Comput. Phys.*, **178**, 210(2002).
2. Wang, Z.J. and Liu, Y.: *J. Comput. Phys.*, **179**, 665(2002).
3. Wang Z.J. and Liu, Y.: *J. of Sci. Comp.*, **20**, 137(2004).
4. Wang, Z.J., Zhang, L. and Liu, Y.: *J. Comput. Phys.*, **194** 716(2004).
5. Godunov, S.K.: *Mat. Sb.* **47**, 271(1959)
6. Cockburn, B., Hou S. and Shu, C.-W.: *Math. of Comp.* **54**, 545(1990).
7. Barth, T.J. and Frederickson, P.O. : AIAA Paper No. 90-0013, 1990.
8. Tam, C.K.W.: *AIAA J.*, **33**, 1788(1995).
9. Shu, C.-W.: *SIAM J. on Sci. and Stat. Comput.* **9**, 1073(1988).
10. Sherer, S. and Visbal, M.: AIAA Paper No. 2003-3203.



(a) Linear SV

(b) Quadratic SV

(c) Cubic SV

Fig. 1. Spectral volumes of various degrees

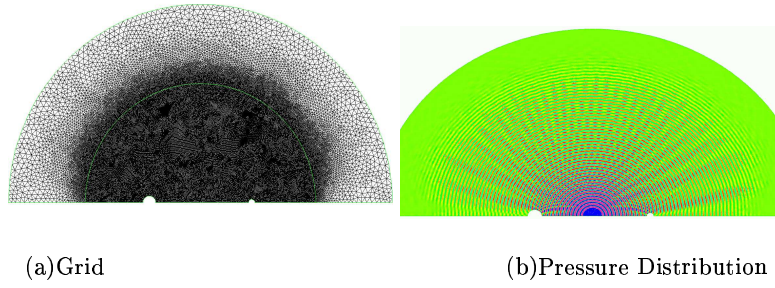


Fig. 2. Computational grid and Pressure Respectively for the two-cylinder diffraction problem

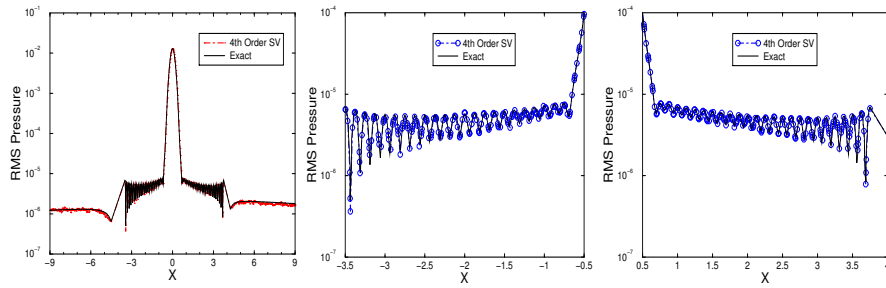


Fig. 3. Comparison of the computational and analytical RMS pressure along the center line

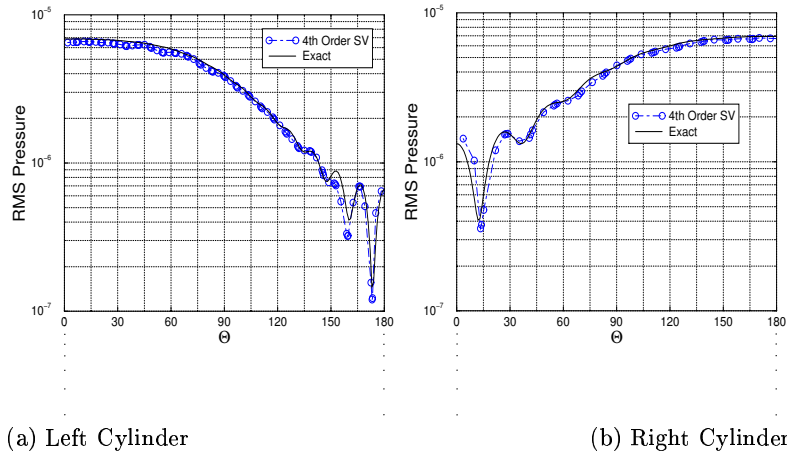


Fig. 4. Comparison of the computational and analytical RMS pressure along the two cylinders

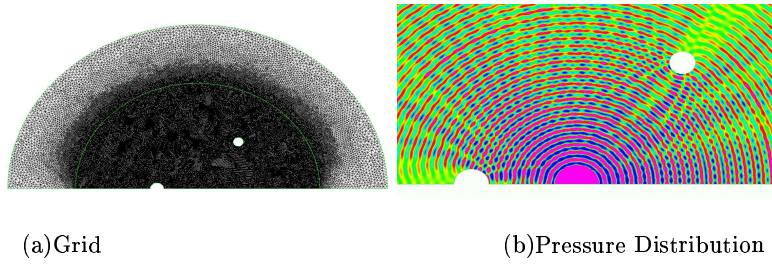


Fig. 5. Pressure distribution computed with the 4th order SV scheme

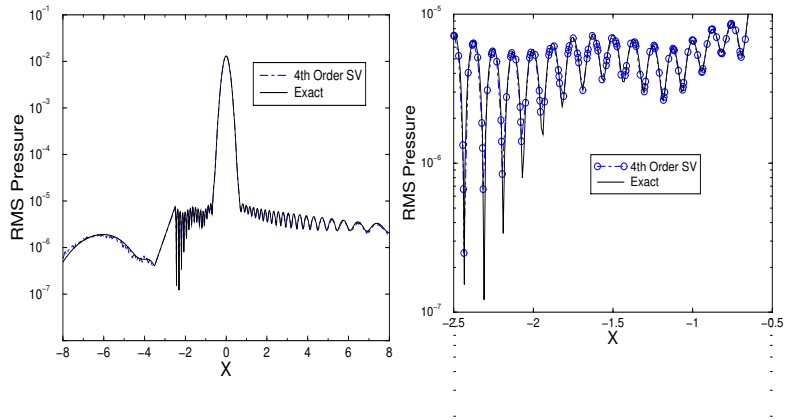


Fig. 6. Comparison of the computational and analytical RMS pressure along the center line

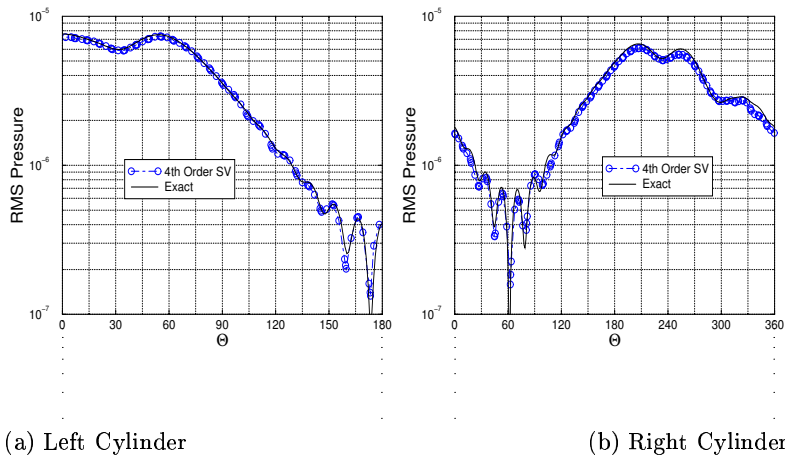


Fig. 7. Comparison of the computational and analytical RMS pressure along the two cylinders